JACS
JOURNAL OF THE AMERICAN CHEMICAL SOCIETY
pubs.acs.org/JACS Article

Tunable Interferometric Effects between Single-Molecule Suzuki−Miyaura Cross-Couplings

Yilin Guo,[§] Chen Yang,[§] Lei Zhang, and Xuefeng Guo*

Cite This: *J. Am. Chem. Soc.* 2023, 145, 6577−6584 Read Online

ACCESS | Metrics & More | Article Recommendations | Supporting Information

Downloaded via PEKING UNIV on April 17, 2023 at 23:51:06 (UTC).
See https://pubs.acs.org/sharingguidelines for options on how to legitimately share published articles.

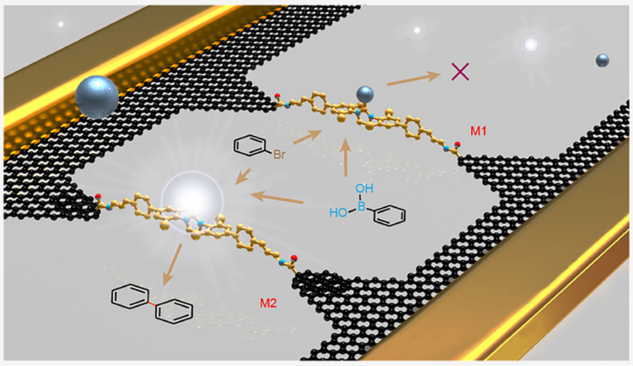

ABSTRACT: Parallel two molecular bridges loaded with a palladium catalyst were integrated into separate pairs of graphene electrodes in the same device. Based on the complete description of the one-palladium catalytic pathway by single-molecule electrical spectroscopy, this setup enables the mapping of the cross-correlation between different catalysts and demonstrates the emergent complexity in the extrapolation from single molecule to ensemble. The anticorrelation behaviors at the time scale of two individual catalysts in sufficiently close proximity were revealed in the Suzuki−Miyaura cross-coupling. Further experimental evidence demonstrates that the long-range electric dipole−dipole interaction induced by solvent leads to the destructive interferometric effect of two catalysts. In contrast, the cooperative coupling of the elementary step between two catalysts affords a local acceleration. This new form of reaction dynamics measurement via focusing on multiple molecules with single-event resolution holds great promise to build a bridge between single molecule and ensemble.

INTRODUCTION

The macroscopic reactive properties are not solely determined by the molecular structure or the single-molecule behavior but by the multiscale hierarchical structure beneath the ensemble.[1−5] In other words, the new reactivities would appear at ascending dimensions, which cannot be predicted by a simple extrapolation from one-molecule behaviors.[6] This leads to plenty of unaddressed but basic issues including the mechanism of self-assembly,[7] the structure of water,[7] the origin of homochirality,[8,9] and even life[7,10] or will.[7] Therein, a formidable challenge is the precise study with multiscales, which necessitates adequate time/spatial resolution and rigorous analysis for a huge interacting network among molecules.

Single-molecule detection (SMD), i.e., focusing on only one molecule without ensemble averaging by optical,[11,12] mechanical,[13,14] or electrical[15,16] approaches, has flourished for several decades. These technologies provide enough resolution and have unveiled a series of inherent properties of the reactions determined by individual molecules, including the hidden intermediates,[17] reaction trajectories,[18] and the autocorrelation behaviors[11,19] at different time scales. However, to further guide the macroscopic synthesis and industrial production, the gap between single molecule and ensemble should be bridged. Following the above train of thought, SMD can be regarded as the starting point to investigate the emergent complexity from bottom to top.[20] One unique example is to measure the polymerization dynamics of one chain, demonstrating the emergent anomalous behaviors accompanied by increased molecular numbers.[13] However, the universal method of measuring the cross-correlation among single-molecule organic reactions and especially the contained elementary step remains a nontrivial task.

To this end, in this study, we adopt the two-dimensional graphene as electrodes to integrate multimolecules to form parallel molecular junctions. The real-time monitoring of the current in the electrical nanocircuit with a constant bias voltage and high-time resolution offers insights into each elementary reaction according to the close relationship between the molecular structure and its conductance.[15,21] In addition, the electrical spectroscopy including the conversion sequence provides a direct observation of the interacting networks among individual catalytic cycles.[19] Therefore, the correlation among molecules during the chemical reaction could be characterized by single molecule/event resolution.

RESULTS AND DISCUSSION

Device Fabrication and Characterization. We take the well-studied Suzuki−Miyaura cross-coupling[18,22,23] as an example (Figure 1A). An open-circuit state with a series of

Received: January 31, 2023
Published: March 14, 2023

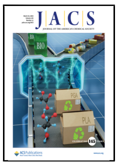

ACS Publications © 2023 American Chemical Society

https://doi.org/10.1021/jacs.3c01108
J. Am. Chem. Soc. 2023, 145, 6577−6584

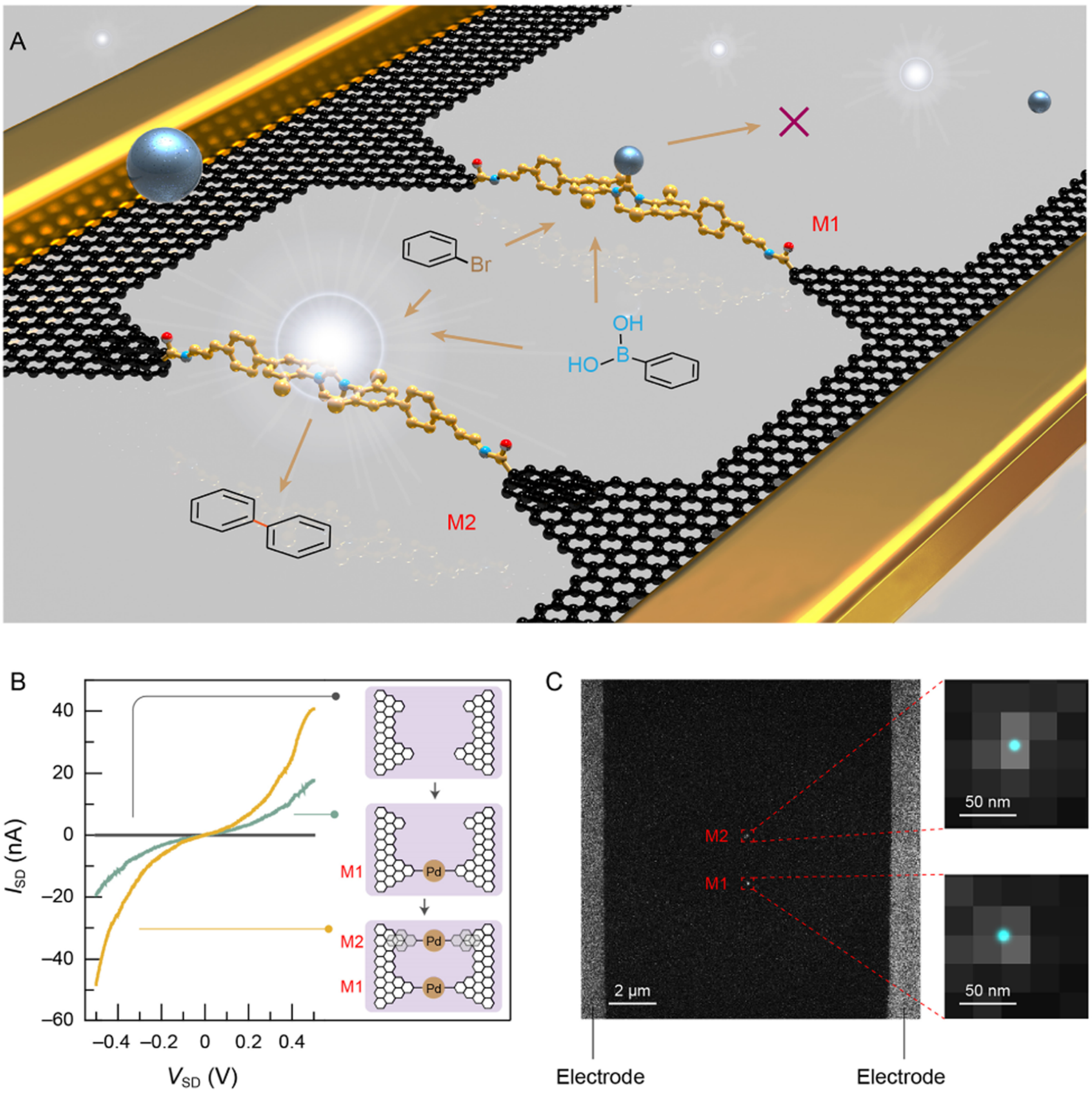

Figure 1. Device structure and characterization of parallel two molecular junctions. (A) Schematic of a parallel two-catalyst device. The top-right molecule (M1) is integrated into the electrodes via covalent bonds, and the bottom-left one (M2) is connected through $\pi-\pi$ stacking. Blue spheres refer to the unreacted Pd catalysts, while bright spheres represent the catalysts under reactions at the same moment. (B) $I-V$ curves of the open circuit with graphene point contacts (black), the single-catalyst junction through covalent connection (green, M1), and the parallel two-catalyst junction (the second molecule was integrated into electrodes via $\pi-\pi$ stacking) (yellow, M1 and M2). I_{SD}, the source−drain current; V_{SD}, the source−drain voltage. (C) Characterization of the parallel connection of two catalysts. The super-high-resolution images of the single-molecule site were obtained by the stochastic optical reconstruction microscopy technology. Laser: 405 nm, 5 mW. Five thousand photos were taken through a ×100 oil lens with an exposure time of 50 ms. In comparison with the corresponding images after integrating the first molecular bridge (Figure S3), the bottom one (M1) is covalently bonded and the top one (M2) is $\pi-\pi$-stacked.

nanogap distributions between carboxyl-terminal graphene electrodes on a SiO_2/Si substrate was obtained by oxygen plasma etching and supplemental electrical burning. A molecular bridge **1** (Scheme S1) containing an NHC−Pd with azido-functionalized side arms (~3.2 nm) was integrated into the suitable gap by the Staudinger ligation[24] and formation of amide-bond interfaces[18] (the molecular synthesis and device fabrication in detail are provided in the Supporting Information, Schemes S1 and S2 and Figures S1 and S2). The recovery of the current−voltage response shows the successful incorporation of the catalyst (Figure 1B). With optimized conditions, the connection yield reached ~17%, with about 29 of the 169 devices on the same silicon chip showing recovery. The statistical analysis in the Supporting Information shows the only-one-molecule connection between the electrodes with an ~92% probability. This was further supported by the super-high-resolution imaging[25] of the single-molecule catalysis, marked as M1 (Figure S3). With the premodification to the terminals with 2-pyrenecarboxylic acid, the elongated molecular bridge **2** (~4.6 nm; Scheme S1) can be further integrated into graphene electrodes again via $\pi-\pi$ stacking with an optimized yield of ~34%. Ten of the above 29 single-molecule devices show the conductance enhancement (Figure 1B). The parallel connection of two catalysts with a series of distance distributions was supported again by the super-high-resolution imaging, marked as M1 and M2 (Figures 1C and 3A). In addition, the detection of the fluorescent product as well as the corresponding fluorescent spectrum (Figure S4) at both sites proves that the reactions on two catalysts proceeded smoothly.

https://doi.org/10.1021/jacs.3c01108
J. Am. Chem. Soc. 2023, 145, 6577−6584

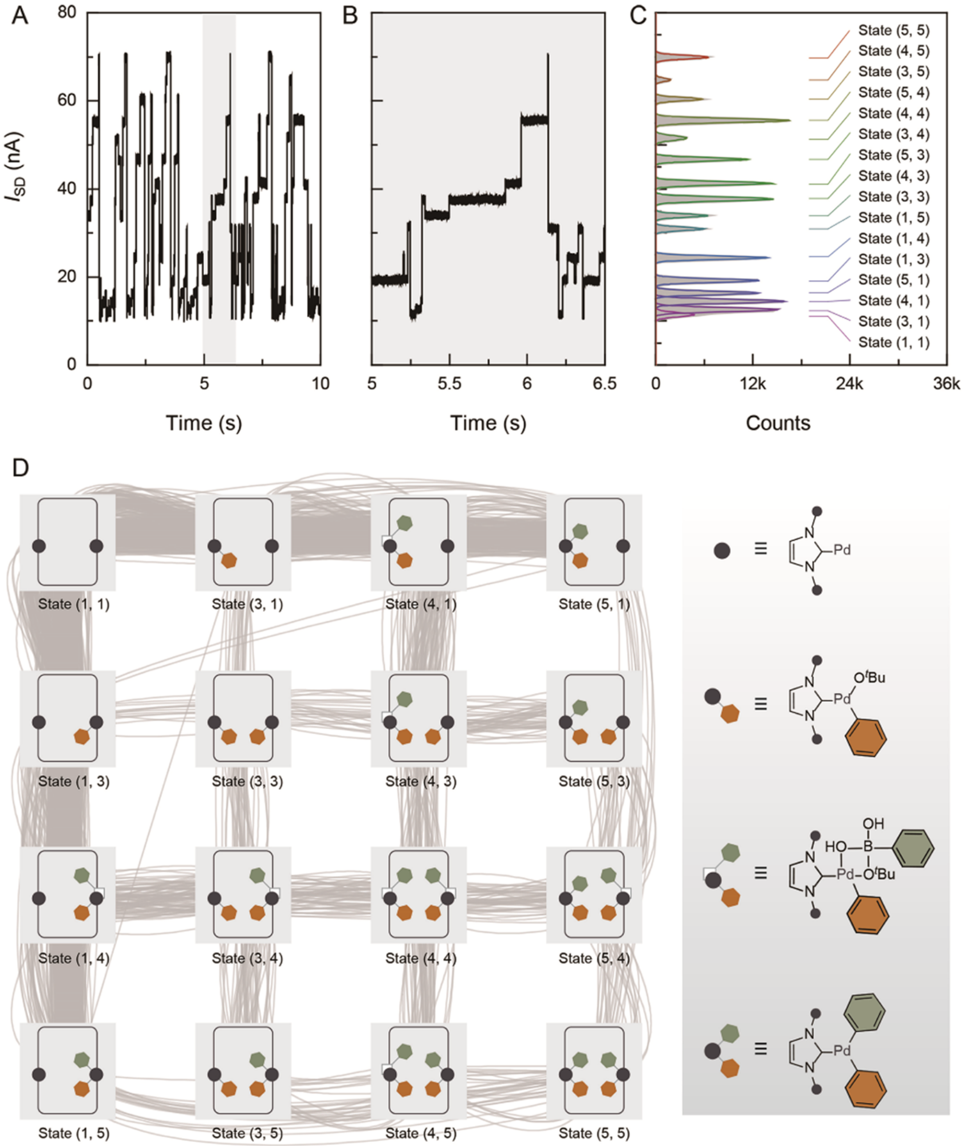

Figure 2. Synchronous electrical characterization of the two catalysts. (A) Recorded I–t curves of the Suzuki–Miyaura cross-coupling with a bias voltage of 300 mV at room temperature. (B) The corresponding enlarged part marked by gray in panel (A). (C) Corresponding histogram of I–t curves shown in panel (A), and the assignments to all of the current states. (D) Left: conversion sequence mapping among the 16 states. The line that connects each state represents a one-time conversion. Right: schematic of four structures during the catalytic cycle.

Synchronous Characterization of the Two Catalysts. Figure 2 shows the synchronous electrical characterization of the two catalysts separated by ~333 nm. With the preactivation by adding a DMF solution of KO^{t}Bu, both the two catalysts formed Pd(0) as the initial state (state (1, 1), ~11.5 nA). The attribution of this state was further supported by the inelastic electron tunneling spectrum (IETS) at 2 K (Figure S5). The subsequent addition of a PhBr solution showed two kinds of stepwise ascents of the current level to state (3, 3) (~34.0 nA), implying the one-by-one oxidative addition of the two Pd(0) (Figure S6). Therein, the inevitable intermediate state (1, 3) (~19.2 nA) or state (3, 1) (~12.5 nA) corresponds to the oxidative addition at only one side. The IETS (Figure S7) of the three species and intermediate-controlled experiments (Figure S8A,B) support that these variations stem from oxidative addition followed by fast ligand exchange. Finally, the addition of $PhB(OH)_2$ led to the periodic conversion of the current level with multiple patterns (involving total 16 states; Figure 2A–C and S9), implying an interacting mode of the catalytic cycle between the two catalysts. Further replacing $PhB(OH)_2$ with the alkylboronic acid blocked the subsequent catalytic progress and stagnated at state (3, 4) (~46.7 nA), state (4, 3) (~37.7 nA), or state (4, 4) (~51.6 nA) (Figure S10). The three states had reversible conversions with state (3, 3), showing the attribution to the pretransmetalation four-membered ring complex located at least on one side. In addition, the vast majority of state (1, 4) (~24.4 nA) and state (4, 1) (~14.8 nA) appeared followed by state (1, 3) and state (3, 1), respectively, in the continuous catalytic cycle and also can be assigned to the pretransmetalation complex at one side and neighboring Pd(0) at the other side. All of the IETSs of these five species show the characteristic peaks of the four-membered ring including the Pd–O–B bond (Figures S11 and S12). The remaining states (state (1, 5), ~31.0 nA; state (3, 5), ~60.4 nA; state (4, 5), ~64.8 nA; state (5, 1), ~16.4 nA; state (5, 3), ~41.3 nA; state

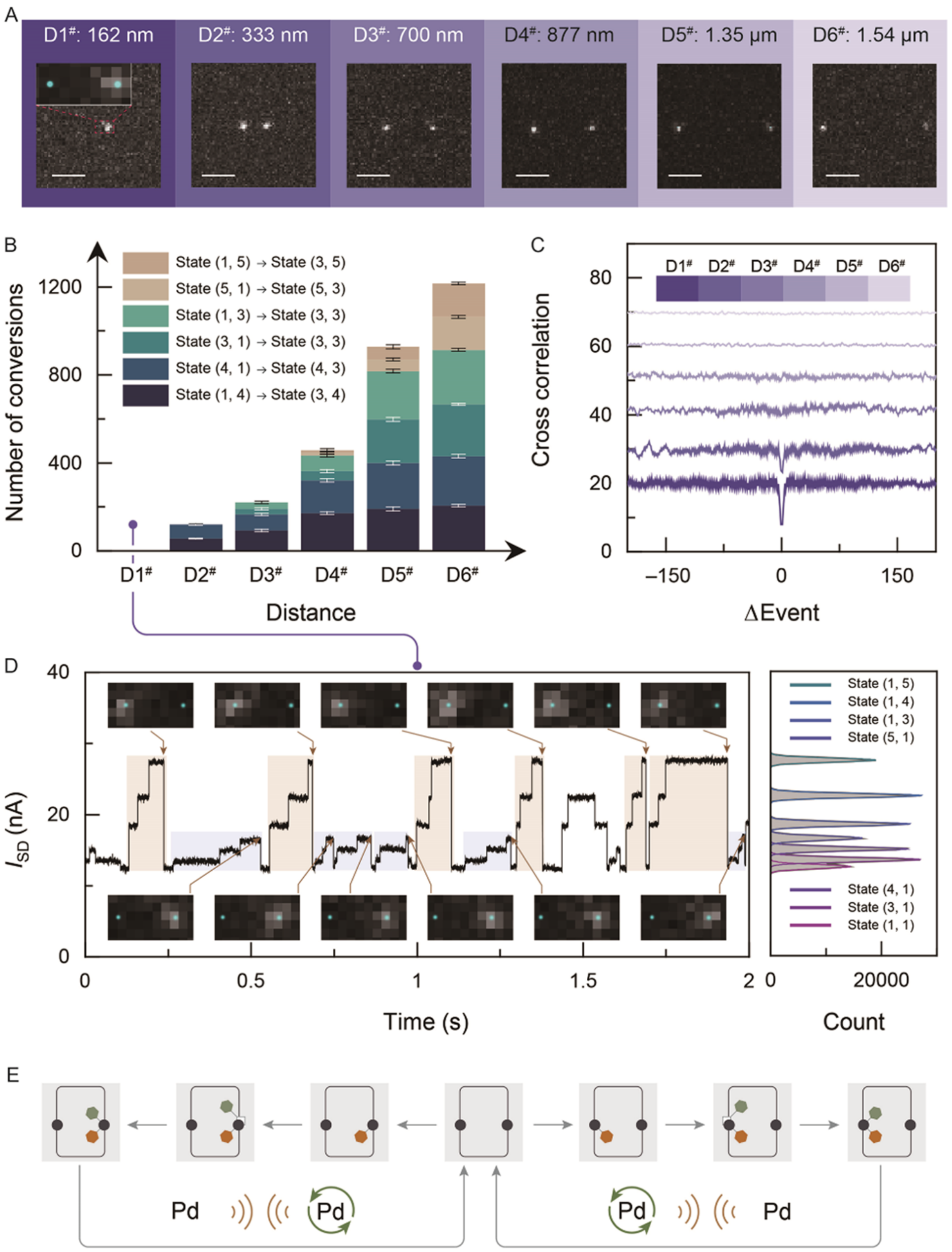

Figure 3. Spatial-distance-dependent measurements of the two catalysts. (A) Super-high-resolution images of the two catalysts with a series of spatial distance distributions between them. Scale bar: 500 nm. The distances between the reconstructed Gaussian-peak centers (the cyan point) are provided on the top. The inset on the left shows the enlarged image, indicating a distance of ∼162 nm. (B) Statistics of the conversion number of each elementary step in the different spatial distances between the two catalysts. (C) Cross-correlation functions between the two catalysts in the spatial-distance-dependent measurements. (D) *I*−*t* curve of the Suzuki−Miyaura cross-coupling with a spatial distance of $D1^{\#}$ = ∼162 nm (left) and the corresponding statistical histogram (right). The super-high-resolution images in the left figure refer to the corresponding reductive elimination elementary step of the two catalysts. The two sites of the catalysts were located via the optical reconstruction and marked as cyan points. The brightness of pixels refers to the fluorescent intensity at the moment, showing an alternative fluorescence emergence at the two sites. (E) Schematic of the destructive interferometric behaviors of the two catalysts.

(5, 4), ∼55.6 nA; and state (5, 5), ∼70.0 nA) can be assigned to the transmetalation complexes located at least on one side by measuring the cross-coupling between 2-acetyl-5-bromothiophene and 4-methoxyphenylboronic acid, where the fluorescence signal of the product was detected following the corresponding states (Figure S13). In addition, the intermediate-controlled experiments (Figure S8C) further support these assignments.

Furthermore, the conversion sequences among all of the 16 states during long-term measurements (100 s; Figure S14B) were mapped in the two-dimensional network, which provided a clear assignment of all of the species by the electrical spectroscopy (Figure 2D). Therein, the line that connects each state represents a one-time conversion. According to this mapping, the anticorrelation of the catalytic behaviors of one catalyst with those of the other catalyst (paused at Pd(0)) was found with a large occupancy, implying a suppression effect of the surrounding catalysts during its working (i.e., Pd(II) state) until rested at state (1, 1), the linkage between the two catalysts at the mapping (Figure 2D, top and left sides). In

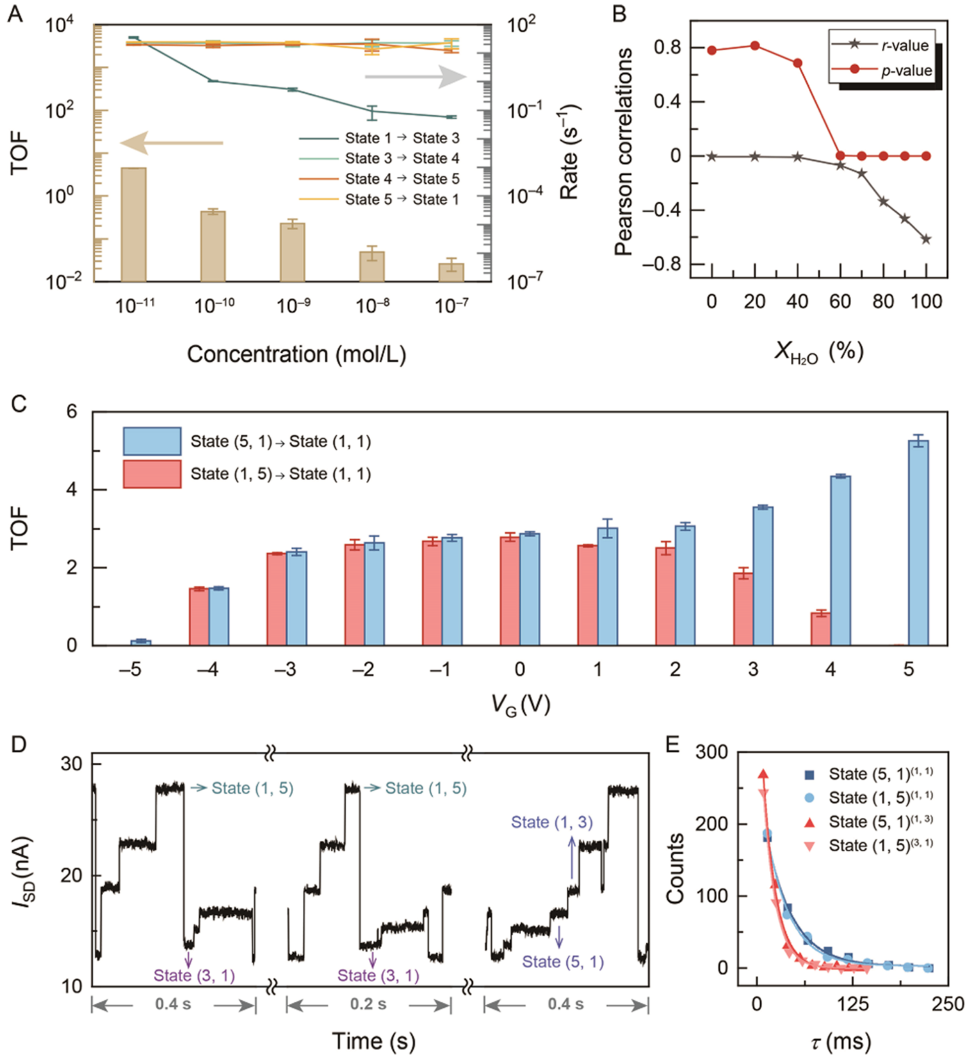

Figure 4. Cross-correlation of the two catalysts. (A) Plots of TOF versus catalyst concentration (bar charts refer to the left-*y*-axis), and rate versus catalyst concentration (line charts refer to the right-*y*-axis) in the external-catalyst-concentration-dependent measurements of the single-catalyst junction. (B) The Pearson cross-correlation analysis of the solvent-dependent two-catalyst behaviors (the distance of two catalysts is ∼162 nm). (C) Statistics of the TOF of two catalysts in the gate-voltage-dependent measurements. (D) Typical *I*−*t* curves of the cooperative coupling between the two catalysts (distance: ∼162 nm). (E) Single-exponential fitting to the distribution of the time intervals of two states in different conditions. State (5, 1)$^{(1, 1)}$ refers to state (5, 1) followed by state (1, 1); state (1, 5)$^{(1, 1)}$ refers to state (1, 5) followed by state (1, 1); state (5, 1)$^{(1, 3)}$ refers to state (5, 1) followed by state (1, 3); state (1, 5)$^{(3, 1)}$ refers to state (1, 5) followed by state (3, 1).

addition, the cross-linked pathways between the above two independent catalytic behaviors were also detected, which specifically originated from the corresponding Pd(II) species and then constructed the whole interacting catalysis network (Figure 2D). Furthermore, the probability of the activation of one Pd(0) at the term of the other's working (at Pd(II)) could also be directly obtained in the mapping (Figure 2D), where the states from high to low are pretransmetalation, ligand exchange, and transmetalation complex. This correlation between the two catalysts can be inferred as an electric dipole−dipole interaction, where the electropositive Pd(II) of one catalyst shows a destructive interferometric effect, i.e., the anticorrelation at time scale on the activation of the other Pd(0). However, this effect is partially quenched by the electron-donating effect from the connected oxygen atom. This will be discussed in detail below.

Cross-Correlation of the Two Catalysts. To demonstrate the detailed two-catalyst behaviors, the electrical spectroscopies of the two catalysts with a series of spatial distance distributions (Figure 3A) were collected (Figure S14). The statistics of each elementary step involved in the interacting network are provided in Figure 3B. With increasing the distance, the crossed pathways between the two catalytic behaviors gradually appeared, which mainly stems from the pretransmetalation complex at arbitrary sides (i.e., state (1, 4) or state (4, 1)), followed by ligand exchange and transmetalation complex sequentially. Essentially equal contributions of these three kinds of conversions were shown in $D6^{\#}$ = ∼1.54 *μ*m, implying totally unrelated behaviors between two catalysts and a random conversion on the catalytic network. This result provides a distance scale of effective correlation between the two catalysts. In addition, the behaviors of the two catalysts were extracted separately according to the electrical signal and the cross-correlation function was used to characterize the relationship between the two catalysts (Figure 3C). A strong anticorrelation (an obvious valley) was obtained at $D1^{\#}$ = ∼162 nm at Δevent = 0, but stochastic dynamics of the elementary step was shown on both the two catalysts at the whole time scale (plateau at Δevent ≠ 0). This strong anticorrelation rapidly vanished at $D3^{\#}$ = ∼700 nm and then transformed into a weak correlation between two catalytic behaviors, constructing the interacting network. Note that the network cannot be formed at the strong anticorrelation condition (Figures 3D−E and S15). For example, the corresponding I−t curve of the coupling between 2-acetyl-5-bromothiophene and 4-methoxyphenylboronic acid is provided in Figure 3D, which shows only two periodic conversion patterns with seven discrete current states (referring to the statistical histogram in the right panel). The characterization by super-high-resolution imaging demonstrated an alternative fluorescence emergence at the two sites (marked with cyan points; Figure 3D). Synchronous electrical signals show that the fluorescence originates from the corresponding reductive elimination elementary step of the two catalysts. This optical evidence further supports these only two anticorrelation catalytic patterns (Figure 3E), i.e., the destructive interferometric behaviors of the two catalysts, which is not favorable for the total turnover.

The electrode-mediated interactions should not be ignored.[26] Instead of integrating the other molecular bridge at the surrounding, i.e., coupled by graphene electrodes, the external addition of Pd(IPr*)(cin)Cl[27] (only the catalytic center) in solution also shows the interferometric effects with the monitored one (the long-term I−t curves of catalyst-concentration-dependent measurements are provided in Figures S16−S18). In combination with the high turnover frequency (TOF) of only one catalyst,[18] the decay versus the increased catalyst concentration shows the through-space destructive interferometric effect (bar charts of Figure 4A), which also provides an extrapolation of the catalysis from single molecule to Avogadro′s number of molecules. Furthermore, the rate of each elementary step was obtained by the maximum interval likelihood estimate,[28] showing an obvious decay of the oxidative addition (line charts of Figure 4A), i.e., the suppression of activating the catalyst. This result supports that the utilization efficiency of the catalysts is the key to the whole TOF in homogeneous catalysis, while a higher TOF of the heterogeneous catalysis, especially the single-atom catalysis,[29] benefits from enough spatial dispersion at least.

In addition, the medium that is able to achieve the interferometric behaviors was studied by solvent-dependent measurements. Acetone and water as well as the mixed solution were adopted to measure the behaviors of the two integrated catalysts with a distance of ∼162 nm (Figure 4B). The corresponding I−t curves are provided in Figure S19, showing a random walking of the two catalysts in pure acetone but less turnover patterns in pure water. The Pearson cross-correlation coefficient was calculated to provide a quantitative analysis of the solvent-dependent two-catalyst behaviors. The more negative r-value (sample correlation coefficient) with increasing the ratio of water shows the enhanced anticorrelation of the two catalysts, while the p-value provides the corresponding significance level. The p-values (<0.05) at the water range of 60−100% support this conclusion. The strong anticorrelation between the two catalysts, i.e., approximated alternative activation at pure DMF or water, implies a long-range electric dipole−dipole interaction[30−32] mediated by these dipolar solvent molecules. This agrees with the long-range orientational organization of these solvents via a dipolar or steric effect.[33] Specifically, the correlation among the acetone molecules was dominated by the steric potentials rather than the electric dipole−dipole interaction due to the two methyl groups located on two sides of the dipole center. The effective electric dipole−dipole interaction could only be constructed by dipolar solvents (such as water). Further control experiments of the MeCN (dipolar solvent)−acetone mixed system support the long-range solvent-mediated electric dipole−dipole interaction between the two catalysts (Figures S20 and S21). It has been noted that although dipolar solvents would contribute to a relatively lower utilization of the catalyst, the influence on each elementary step as well as solubility should also be considered to select a suitable solvent in the macroscopic synthesis.

The regulation of the cross-correlation between the two catalysts can be achieved by controlling its valence state through the gate voltage,[34] which further supported the solvent-mediated long-range electric dipole−dipole interaction. With the applied gate voltage from the back Si substrate, one catalyst shows an obvious limitation to Pd(0) (positive gate) or Pd(II) (negative gate), while the other proceeds smoothly (the corresponding I−t curves are provided in Figures S22−S27). In combination with the distinction of the two molecular junctions by the super-high-resolution optical imaging (Figure S28), the gate-voltage-independent one should be assigned to the π−π-stacked catalyst and the other is covalently bonded (the detailed optical images and electrical signals of two catalysts at V_G = +5 V (−5 V) are provided in Figure S29, which shows that the π−π-stacked catalyst is gate-voltage-independent, while the covalently bonded catalyst is not). This difference may originate from the pinning of the π−π-stacked catalyst to the Fermi energy level and the shield of the gate field by graphene electrodes. In this particular condition, the long-range interferometric effects from the valence-state-controlled covalently bonded catalyst to the target π−π-stacked catalyst can be monitored with a long-time scale. As shown in Figure 4C, in comparison with the behaviors at V_G = 0 V, the limited Pd(0) (Pd(II)) has a positive (negative) influence on the neighboring catalyst at V_G = +5 V (−5 V), which is in consistence with the above results. The modulation of only one and the observation of all of the molecules highlight the capability of the multiple-molecule junctions to study the molecular collective behaviors and the emergent complexity, therefore providing a possibility of guiding the trend of the whole reaction.

In addition to the destructive interferometric effects between the two catalysts, the cooperative coupling between them was also detected in sufficiently close proximity, e.g., $D2^{\#}$ = ∼333 nm and $D1^{\#}$ = ∼162 nm. Specifically, the activation of one catalyst occasionally promoted the other to undergo reductive elimination and generated a cross-coupled product. Note that it is also in line with the anticorrelation behaviors. Here, the oxidative addition of one catalyst and the reductive elimination of the other show a nearly concerted process and the state (1, 1) intermediate cannot be detected with the ∼17 μs time resolution. For example, both the direct conversions from state (1, 5) to (3, 1) and (5, 1) to (1, 3) (not linked by state (1, 1)) were found at $D2^{\#}$ = ∼333 nm (refer to the statistical network in Figure 2D) and $D1^{\#}$ = ∼162 nm (refer to the typical I−t curves in Figure 4D). In addition, the dwell time of state (1, 5) (state (5, 1)) followed by state (1, 1) and state (3, 1) (state (1, 3)) was extracted, respectively. The single-exponential fitting to the distribution of the time intervals provides the corresponding characteristic lifetime (Figure 4E), which represents the difference between the stepwise (blue line) and concerted (red line) reaction dynamics. The lifetime of the transmetalation complex followed by the stepwise process (denoted as state $(5, 1)^{(1, 1)}$ and state $(1, 5)^{(1, 1)}$) was obtained as 34.7 ± 1.5 and 30.9 ± 2.1 ms, respectively. While the shorter lifetime of state $(5, 1)^{(1, 3)}$ (17.3 ± 1.0 ms) and state $(1, 5)^{(3, 1)}$ (16.1 ± 0.7 ms) followed by the concerted process implies a coupled acceleration between the two catalysts. In addition, a similar statistical lifetime was found in the two catalysts at the same conversion pattern, which shows equal reactivity and excludes the influence of integration with the different interfaces. Considering the relatively lower occupancy of the concerted way, this cooperative coupling could only provide a local acceleration in the whole reaction. In combination with the destructive interferometric effects, a comprehensive study of the collective-catalyst reaction dynamics is a challenge, but a derived opportunity is that a rational design of the catalyst system may contribute to a controllable reaction dynamic as well as maximize the utilization efficiency and atom economy.

CONCLUSIONS

The parallel multimolecular junctions with variant distances enable the characterization of the emergent complexity from one to two molecules in catalysis. The destructive interferometric behaviors were detected statistically between the two catalysts in sufficiently close proximity (∼162 nm) via the long-range electric dipole−dipole interaction mediated by dipolar solvents, which could contribute to a lower TOF at macroscopic experiments. Meanwhile, a local acceleration stemming from the cooperative coupling between the catalysts also exists, showing complex dynamic characteristics in the intrinsic Suzuki−Miyaura cross-coupling at the macroscopic level. The destructive interferometric effects and cooperative coupling between the catalytic behaviors expand our knowledge of the mechanism and potentially provide guidance to optimize the macroscopic reaction conditions. Totally bridging the gap between single molecule and ensemble requires more comprehensive single-molecule/single-event-resolved characterization and powerful analysis technologies.

ASSOCIATED CONTENT

Supporting Information

The Supporting Information is available free of charge at https://pubs.acs.org/doi/10.1021/jacs.3c01108.

> Molecular synthesis, fabrication procedures of graphene field-effect transistor (FET) arrays and molecular junctions, single-molecule connection analysis, fluorescent super-resolution imaging of the only-one-molecule junction, fluorescent spectra of the product, characterizations of different states in the two-catalyst Suzuki−Miyaura cross-coupling, spatial-distance-dependent measurements of the two-catalyst junction, conversion sequence mapping at the strong anticorrelation condition, catalyst-concentration-dependent measurements of the one-catalyst junction, solvent-dependent measurements of the two-catalyst junction, gate-voltage-dependent measurements of the two-catalyst junction, and references (PDF)

AUTHOR INFORMATION

Corresponding Author

Xuefeng Guo − *Beijing National Laboratory for Molecular Sciences, National Biomedical Imaging Center, College of Chemistry and Molecular Engineering, Peking University, Beijing 100871, P. R. China; Center of Single-Molecule Sciences, Institute of Modern Optics, Frontiers Science Center for New Organic Matter, College of Electronic Information and Optical Engineering, Nankai University, Tianjin 300350, P. R. China;* orcid.org/0000-0001-5723-8528; Email: guoxf@pku.edu.cn

Authors

Yilin Guo − *Beijing National Laboratory for Molecular Sciences, National Biomedical Imaging Center, College of Chemistry and Molecular Engineering, Peking University, Beijing 100871, P. R. China*

Chen Yang − *Beijing National Laboratory for Molecular Sciences, National Biomedical Imaging Center, College of Chemistry and Molecular Engineering, Peking University, Beijing 100871, P. R. China*

Lei Zhang − *Beijing National Laboratory for Molecular Sciences, National Biomedical Imaging Center, College of Chemistry and Molecular Engineering, Peking University, Beijing 100871, P. R. China;* orcid.org/0000-0001-9031-4318

Complete contact information is available at: https://pubs.acs.org/10.1021/jacs.3c01108

Author Contributions

[§]Y.G. and C.Y. contributed equally to this work.

Notes

The authors declare no competing financial interest.

ACKNOWLEDGMENTS

The authors acknowledge the primary financial support from the National Key R&D Program of China (2021YFA1200101 and 2022YFE0128700), the National Natural Science Foundation of China (22150013, 21933001, and 21727806), the Tencent Foundation through the XPLORER PRIZE, and the Natural Science Foundation of Beijing (2222009).

REFERENCES

(1) Anderson, P. W. More is different: Broken symmetry and nature of hierarchical structure of science. *Science* **1972**, *177*, 393−396.

(2) Strogatz, S.; Walker, S.; Yeomans, J. M.; Tarnita, C.; Arcaute, E.; De Domenico, M.; Artime, O.; Goh, K.-I. Fifty years of 'More is different. *Nat. Rev. Phys.* **2022**, *4*, 508−510.

(3) Ottino, J. M. Engineering complex systems. *Nature* **2004**, *427*, 399.

(4) Hartwell, L. H.; Hopfield, J. J.; Leibler, S.; Murray, A. W. From molecular to modular cell biology. *Nature* **1999**, *402*, C47−C52.

(5) Crutchfield, J. P. Between order and chaos. *Nat. Phys.* **2012**, *8*, 17−24.

(6) Wang, H.; Park, M.; Dong, R.; Kim, J.; Cho, Y. K.; Tlusty, T.; Granick, S. Boosted molecular mobility during common chemical reactions. *Science* **2020**, *369*, 537−541.

(7) American Association for the Advancement of Science. So much more to know···. *Science* **2005**, *309*, 78−102.

(8) Jafarpour, F.; Biancalani, T.; Goldenfeld, N. Noise-induced mechanism for biological homochirality of early life self-replicators. *Phys. Rev. Lett.* **2015**, *115*, No. 158101.

(9) Piñeros, W. D.; Tlusty, T. Spontaneous chiral symmetry breaking in a random driven chemical system. *Nat. Commun.* **2022**, *13*, No. 2244.

(10) Marshall, S. M.; Mathis, C.; Carrick, E.; Keenan, G.; Cooper, G. J. T.; Graham, H.; Craven, M.; Gromski, P. S.; Moore, D. G.; Walker, S. I.; Cronin, L. Identifying molecules as biosignatures with assembly theory and mass spectrometry. *Nat. Commun.* **2021**, *12*, No. 3033.

(11) Lu, H. P.; Xun, L. Y.; Xie, X. S. Single-molecule enzymatic dynamics. *Science* **1998**, *282*, 1877−1882.

(12) Zrimsek, A. B.; Chiang, N.; Mattei, M.; Zaleski, S.; McAnally, M. O.; Chapman, C. T.; Henry, A. I.; Schatz, G. C.; Van Duyne, R. P. Single-molecule chemistry with surface- and tip-enhanced Raman spectroscopy. *Chem. Rev.* **2017**, *117*, 7583−7613.

(13) Liu, C. M.; Kubo, K. R.; Wang, E. D.; Han, K. S.; Yang, F.; Chen, G. Q.; Escobedo, F. A.; Coates, G. W.; Chen, P. Single polymer growth dynamics. *Science* **2017**, *358*, 352−355.

(14) Lussis, P.; Svaldo-Lanero, T.; Bertocco, A.; Fustin, C. A.; Leigh, D. A.; Duwez, A. S. A single synthetic small molecule that generates force against a load. *Nat. Nanotechnol.* **2011**, *6*, 553−557.

(15) Li, Y.; Yang, C.; Guo, X. Single-molecule electrical detection: A promising route toward the fundamental limits of chemistry and life science. *Acc. Chem. Res.* **2020**, *53*, 159−169.

(16) Branton, D.; Deamer, D. W.; Marziali, A.; Bayley, H.; Benner, S. A.; Butler, T.; Di Ventra, M.; Garaj, S.; Hibbs, A.; Huang, X.; Jovanovich, S. B.; Krstic, P. S.; Lindsay, S.; Ling, X. S.; Mastrangelo, C. H.; Meller, A.; Oliver, J. S.; Pershin, Y. V.; Ramsey, J. M.; Riehn, R.; Soni, G. V.; Tabard-Cossa, V.; Wanunu, M.; Wiggin, M.; Schloss, J. A. The potential and challenges of nanopore sequencing. *Nat. Biotechnol.* **2008**, *26*, 1146−1153.

(17) Yang, C.; Liu, Z.; Li, Y.; Zhou, S.; Lu, C.; Guo, Y.; Ramirez, M.; Zhang, Q.; Li, Y.; Liu, Z.; Houk, K. N.; Zhang, D.; Guo, X. Electric field−catalyzed single-molecule Diels-Alder reaction dynamics. *Sci. Adv.* **2021**, *7*, No. eabf0689.

(18) Yang, C.; Zhang, L.; Lu, C.; Zhou, S.; Li, X.; Li, Y.; Yang, Y.; Li, Y.; Liu, Z.; Yang, J.; Houk, K. N.; Mo, F.; Guo, X. Unveiling the full reaction path of the Suzuki−Miyaura cross-coupling in a single-molecule junction. *Nat. Nanotechnol.* **2021**, *16*, 1214−1223.

(19) Yang, C.; Zhang, L.; Li, H.; Guo, Y.; Jia, C.; Zhu, W.; Mo, F.; Guo, X. Single-molecule electrical spectroscopy of organocatalysis. *Matter* **2021**, *4*, 2874−2885.

(20) Guo, Y.; Yang, C.; Jia, C.; Guo, X. Accurate single-molecule indicator of solvent effects. *JACS Au* **2021**, *1*, 2271−2279.

(21) Aviram, A.; Ratner, M. A. Molecular rectifiers. *Chem. Phys. Lett.* **1974**, *29*, 277−283.

(22) Miyaura, N.; Yanagi, T.; Suzuki, A. The palladium-catalyzed cross-coupling reaction of phenylboronic acid with haloarenes in the presence of bases. *Synthetic Commun.* **1981**, *11*, 513−519.

(23) Lennox, A. J. J.; Lloyd-Jones, G. C. Transmetalation in the Suzuki−Miyaura coupling: The fork in the trail. *Angew. Chem., Int. Ed.* **2013**, *52*, 7362−7370.

(24) Kosal, A. D.; Wilson, E. E.; Ashfeld, B. L. Phosphine-based redox catalysis in the direct traceless Staudinger ligation of carboxylic acids and azides. *Angew. Chem., Int. Ed.* **2012**, *51*, 12036−12040.

(25) Rust, M. J.; Bates, M.; Zhuang, X. Sub-diffraction-limit imaging by stochastic optical reconstruction microscopy (STORM). *Nat. Methods* **2006**, *3*, 793−795.

(26) Li, Q. K.; Li, X. F.; Zhang, G. Z.; Jiang, J. Cooperative spin transition of monodispersed FeN_3 sites within graphene induced by CO adsorption. *J. Am. Chem. Soc.* **2018**, *140*, 15149−15152.

(27) Marion, N.; Navarro, O.; Mei, J.; Stevens, E. D.; Scott, N. M.; Nolan, S. P. Modified (NHC)Pd(allyl)Cl (NHC = N-heterocyclic carbene) complexes for room-temperature Suzuki−Miyaura and Buchwald−Hartwig reactions. *J. Am. Chem. Soc.* **2006**, *128*, 4101−4111.

(28) Milescu, L. S.; Yildiz, A.; Selvin, P. R.; Sachs, F. Maximum likelihood estimation of molecular motor kinetics from staircase dwell-time sequences. *Biophys. J.* **2006**, *91*, 1156−1168.

(29) Qiao, B. T.; Wang, A. Q.; Yang, X. F.; Allard, L. F.; Jiang, Z.; Cui, Y. T.; Liu, J. Y.; Li, J.; Zhang, T. Single-atom catalysis of CO oxidation using Pt-1/FeOx. *Nat. Chem.* **2011**, *3*, 634−641.

(30) Luo, Z. L.; Xiao, H. Y.; Peng, X. C.; Li, Y. L.; Zhu, Z. P.; Tian, Y.; Jiang, L. Long-range ordered water correlations between A-T/C-G nucleotides. *Matter* **2020**, *3*, 794−804.

(31) Nardecchia, I.; Lechelon, M.; Gori, M.; Donato, I.; Preto, J.; Floriani, E.; Jaeger, S.; Mailfert, S.; Marguet, D.; Ferrier, P.; Pettini, M. Detection of long-range electrostatic interactions between charged molecules by means of fluorescence correlation spectroscopy. *Phys. Rev. E* **2017**, *96*, No. 022403.

(32) Kurian, P.; Capolupo, A.; Craddock, T. J. A.; Vitiello, G. Water-mediated correlations in DNA-enzyme interactions. *Phys. Lett. A* **2018**, *382*, 33−43.

(33) Duboisset, J.; Rondepierre, F.; Brevet, P. F. Long-range orientational organization of dipolar and steric liquids. *J. Phys. Chem. Lett.* **2020**, *11*, 9869−9875.

(34) Zhang, L.; Yang, C.; Lu, C. X.; Li, X. X.; Guo, Y. L.; Zhang, J. N.; Lin, J. L.; Li, Z. Z.; Jia, C. C.; Yang, J. L.; Houk, K. N.; Mo, F. Y.; Guo, X. F. Precise electrical gating of the single-molecule Mizoroki-Heck reaction. *Nat. Commun.* **2022**, *13*, No. 4552.

Recommended by ACS

Directing Group Repositioning Strategy Enabled Site- and Enantioselective Addition of Heteroaromatic C–H Bonds to Acyclic Internal Alkenes

Wei Zhao and Bi-Jie Li

MARCH 14, 2023

JOURNAL OF THE AMERICAN CHEMICAL SOCIETY

READ

Molecular Bridge Engineering for Tuning Quantum Electronic Transport and Anisotropy in Nanoporous Graphene

César Moreno, Aitor Mugarza, *et al.*

MARCH 29, 2023

JOURNAL OF THE AMERICAN CHEMICAL SOCIETY

READ

Iminyl-Radical-Mediated Formation of Covalent Au–N Bonds for Molecular Junctions

Mingliang Zhang, Daoben Zhu, *et al.*

MARCH 07, 2023

JOURNAL OF THE AMERICAN CHEMICAL SOCIETY

READ

Dual Ruthenium-Catalyzed Alkene Isomerization–Hydrogen Auto-Transfer Unlocks Skipped Dienes as Pronucleophiles for Enantioselective Alcohol C–H Allylation

Zachary J. Dubey, Michael J. Krische, *et al.*

APRIL 05, 2023

JOURNAL OF THE AMERICAN CHEMICAL SOCIETY

READ

Get More Suggestions >